A simple model for longitudinal electron transport during and after laser excitation: Emergence of electron resistive transport

Robert Meadows

Department of Physics, Indiana State University, Terre Haute, IN 47809, USA

Y. Xue

Milwaukee Area Technical College, Milwaukee, WI 53233-1443, USA

Nicholas Allbritton and G. P. Zhang*

Department of Physics, Indiana State University, Terre Haute, IN 47809

(Dated: December 9, 2024)

Laser-driven electron transport across a sample has garnered enormous attentions over several decades, as it provides a much faster way to control electron dynamics. Light is an electromagnetic wave, so how and why an electron can acquire a longitudinal velocity remains unanswered. Here we show that it is the magnetic field that steers the electron to the light propagation direction. But, quantitatively, our free-electron model is still unable to reproduce the experimental velocities. Going beyond the free electron mode and assuming the system absorbs all the photon energy, the theoretical velocity matches the experimental observation. We introduce a concept of the resistive transport, where electrons deaccelerate under a constant resistance after laser excitation. This theory finally explains why the experimental distance-versus-time forms a down-concave curve, and unifies ballistic and superdiffusive transports into a single resistive transport. We expect that our finding will motivate further investigations.

I. INTRODUCTION

Electron transport is a common phenomenon that occurs in various forms. An electron can diffuse under a temperature or concentration gradient, often described by the diffusion equation [1], $\frac{\partial n}{\partial t} = D\frac{\partial^2 n}{\partial z^2} - \frac{n}{T}$, where n is the electron density, D is the diffusion constant and T is the relaxation time. If an electric field is applied, one can describe it through the Boltzmann equation [2, 3], $\frac{\partial f}{\partial t} + \mathbf{v}\cdot\frac{\partial f}{\partial \mathbf{r}} + \frac{e\mathbf{E}}{m_e}\cdot\frac{\partial f}{\partial \mathbf{v}} = -\frac{f-f_0}{T}$, where f is the electron distribution function, $\mathbf{v}$ is the electron velocity, $\mathbf{r}$ is its position, m_e is the electron mass, and $\mathbf{E}$ is the electric field. When one applies a voltage bias along the x axis across a device, the electron inside the device moves along the x axis. This is how classical physics explains electron transport. When the device becomes shorter, one has a ballistic transport, where the electron travels like a bullet without resistance inside the device [4]. Now, consider a linearly-polarized laser pulse, propagating along the z axis and with its electric field $\mathbf{E}$ along the x axis and the magnetic field $\mathbf{B}$ along the y axis, is applied on to the same device (Fig. 1). It is obvious that the electron will move along the x axis, since $\mathbf{E}$ is along the x. But there is no electric field along the z axis. So does the electron travel along the longitudinal direction?

The answer is affirmative. In 1987, Brorson et al. [5] employed a 96-fs laser pump pulse of wavelength 630 nm and of fluence 1 mJ/cm² to excite a group of thin gold films of thickness from 200 to 3000 Å from the front, and then detected the reflected probe beam from the back of the sample. They found that the electron can travel at 10^8 cm/s, very close to the Fermi velocity of electrons in Au. In 2011, Melnikov et al. [6] employed the same experimental setup, but with a magnetic film Au/Fe/MgO(001), where the thickness of Fe is 15 nm and that of Au is 50 and 100 nm. They sent in a p-polarized 35-fs pump pulse of 800 nm on to the Fe layer through the MgO substrate, and then detected the magnetic second-harmonic (MSH) signal reflected from the back of the Au layer. They found the MSH hysteresis loop after 30 fs delay between the pump and probe, even with fluence 1 mJ/cm² and energy 40 nJ per pulse. These results attracted a broad interest [7–14]. Besides MSH, Beyazit et al. [15, 16] employed the time-resolved two-photon photoemission and found that the electron lifetimes are shorter when the thickness of their Au layer increases. They concluded the excited electrons propagate through Au in a superdiffusive regime [17], but ballistically across the interfaces. The transition from a superdiffusive to a diffusive transport occurs around 20-30 nm of the Au layer [18]. Using the same technique, Bühlmann et al. [19] detected 4% spin polarization change in the Au film, consistent with that of Hofherr et al. [11]. Recently, Karna et al. [20] reported that the ballistic length of hot electrons in gold films exceeds 150 nm, 50% larger than 100 nm from prior studies. But their experimental geometry is different. They measured the lateral motion (along the traverse direction), not along the longitudinal direction [5, 21].

Theoretically, several models are proposed. Salvatella et al. [22] proposed the analytical model of the demagnetization amplitude, where they linked the absorbed energy to the temperature change and then to the demagnetization. Another one is the superdiffusion model [17], where one assumes a time-dependent diffusion exponent and then solves the diffusion equation for the electron. These theories build in a gradient from the beginning,

but how such a gradient is established is not addressed. This boils down to the fundamental question: why and how the electron could gain the longitudinal velocity [23–25]. In atoms and plasma physics, a similar problem has been studied before [26, 27], but with the laser fluence over 2×10^5 J/cm^2, which has little relevance to laser-induced electron transport in a real device.

Given the complexity of the problem [28], we have two moderate objectives. First, we limit ourselves to a simpler question: Is it possible to understand laser-induced electron transport qualitatively using a free-electron model? We employ Varga and Török's method, which is based on the Hertz vector. We carry out a series of simulations by solving the Newtonian equation of motion of the electron. We find that the longitudinal velocity is a joint effect of the electric and magnetic fields of the laser pulse. However, using the same experimental laser parameters [29], we are still unable to quantitatively reproduce the experimental results. Going beyond the free electron model and assuming all the photon energy absorbed into the system, we find that the electron velocity then matches the experimental ones. Second, after laser excitation, we introduce a new concept of the resistive transport, where hot electrons deaccelerate under a constant resistance from other electrons and ions. This does not only explain why experimentally [30, 31] the dependence of the electron time on the electron distance is a down concave, but also unifies the ballistic transport [32, 33] and the superdiffusive transport [17] as a single resistive transport. Our finding will have an important impact on the future investigation of ultrafast electron and spin transport [5, 6, 34–36].

The rest of the paper is arranged as follows. Section II is devoted to our theoretical formalism. Numerical results during the laser excitation are given in Sec. III, where we compare our results with the Compton scattering and the experimental results. In Sec. IV, we compare and contrast four models with the latest experimental data. Section V introduces the resistive transport theory after the initial excitation. We conclude this paper in Sec. VI.

II. FORMALISM

We consider a free electron placed inside a laser field, with its electric-field $\mathbf{E}$ along the x axis and the magnetic field $\mathbf{B}$ along the y axis. Figure 1(a) schematically illustrates a typical experimental geometry, where the laser pulse propagates toward the sample along the z axis. The Hamiltonian of the electron inside an electromagnetic field is

$$H = \frac{1}{2m}(\mathbf{p} - q\mathbf{A}(\mathbf{r}, t))^2 + q\phi, \tag{1}$$

where $\mathbf{A}(\mathbf{r}, t)$ is the vector potential, ϕ is the scalar potential, m and q are the electron mass and charge, respectively. The equation of motion is given in terms of the generalized Lorentz force as [37],

$$m\frac{d^2\mathbf{r}}{dt^2} = q\mathbf{E}(\mathbf{r}, t) + \frac{q}{2m}(\mathbf{p} \times \mathbf{B}(\mathbf{r}, t) - \mathbf{B}(\mathbf{r}, t) \times \mathbf{p}) - \frac{q^2}{m}(\mathbf{A}(\mathbf{r}, t) \times \mathbf{B}(\mathbf{r}, t)). \tag{2}$$

If we set $\mathbf{B}(\mathbf{r}, t)$ to zero, then every term, except the first term, on the right side, is zero, so the electron only moves along $\mathbf{E}(\mathbf{r}, t)$. This demonstrates that it is indispensable to include $\mathbf{B}(\mathbf{r}, t)$.

We follow Varga and Török [38], and start from the Hertz vector, which satisfies the vectorial Helmholtz equation, so the resultant electric and magnetic fields automatically satisfy the Maxwell equation, given in an integral form. Within the paraxial approximation, we get the reduced $\tilde{\mathbf{E}}$ and $\tilde{\mathbf{B}}$,

$$\tilde{E}_x = \left[1 + \frac{4x^2 - 2w_0^2}{w_0^4 k^2}\right], \quad \tilde{E}_y = \frac{4xy}{w_0^4 k^2}, \quad \tilde{E}_z = -\frac{2ik_z x}{w_0^2 k^2}.$$
$$\tilde{B}_x = 0, \qquad \tilde{B}_y = -\frac{ik_z\sqrt{\epsilon\mu}}{k}, \quad \tilde{B}_z = -\frac{2y\sqrt{\epsilon\mu}}{kw_0^2}. \tag{3}$$

The final electric and magnetic fields are

$$\mathbf{E} = A_0\tilde{\mathbf{E}}e^{ik_z z - i\omega t - \left(\frac{x^2 + y^2}{w_0^2}\right)}, \mathbf{B} = A_0\tilde{\mathbf{B}}e^{ik_z z - i\omega t - \left(\frac{x^2 + y^2}{w_0^2}\right)}, \tag{4}$$

where A_0 is the field amplitude and w_0 is the pulse spatial width chosen as 10λ. λ is the wavelength of the pulse.

When the light enters a sample, both fields are reduced by $e^{-z/(2\lambda_{pen})}$, where λ_{pen} is the penetration depth and 2 comes from the fact that penetration depth is defined at $1/e$ the incident fluence and the fluence is proportional to the square of the electric field. λ_{pen} is chosen to be 14 nm, typically values in fcc Ni.

In our study, we choose a linearly x-polarized pulse that is propagating along the z axis. The pulse is a Gaussian of duration τ, amplitude A_0 and photon energy $h\nu$. $A_0 e^{-i\omega t}$ in $\mathbf{E}$ and $\mathbf{B}$ in Eq. 4 is replaced by $A_0 e^{-t^2/\tau^2}\cos(\omega t)$, so our electric and magnetic fields are

$$\mathbf{E}(\mathbf{r}, t) = A_0 e^{-t^2/\tau^2}\cos(\omega t)\tilde{\mathbf{E}}e^{ik_z z - \frac{z}{2\lambda_{pen}} - \left(\frac{x^2 + y^2}{w_0^2}\right)}, \tag{5}$$

$$\mathbf{B}(\mathbf{r}, t) = A_0 e^{-t^2/\tau^2}\cos(\omega t)\tilde{\mathbf{B}}e^{ik_z z - \frac{z}{2\lambda_{pen}} - \left(\frac{x^2 + y^2}{w_0^2}\right)}, \tag{6}$$

These analytic forms of $\mathbf{E}$ and $\mathbf{B}$, which contain both the spatial and temporal dependences, greatly ease our calculation. As a first step toward a complete transport theory, we treat the electron classically, and solve the

Newtonian equation of motion numerically,

$$\frac{d\mathbf{v}}{dt} = \frac{q}{m}\left[\mathbf{E}(\mathbf{r}, t) + \mathbf{v} \times \mathbf{B}(\mathbf{r}, t)\right], \qquad (7)$$

where $\mathbf{v}$ is the electron velocity. Although our method is classical, it fully embraces the real space approach that is more suitable for transport, a key feature that is often missing from prior first-principles and model simulations. This will answer the most critical question why the electron can move along the axial direction.

III. DURING LASER EXCITATION

We start with the experimental laser parameters from Razdolski *et al.* [29], where their laser fluence is $F = 10$ mJ/cm^2, duration $\tau = 14$ fs, and photon energy of $h\nu = 1.55$ eV. These parameters are typically used in experiments [39]. We use [40] $F = \frac{1}{2}cn\epsilon_0|A_0|^2\sqrt{\frac{\pi}{2}}\tau$ to find the electric field amplitude to be $A_0 = 0.207$ V/Å. Our electric field is shown in Fig. 2(a). The initial position and velocity of the electron are set to zero. Figure 2(b) shows the velocity v_x and position x oscillate strongly with time. The maximum velocity reaches 1.5 Å/fs, 1.5×10^5 m/s, on the same order of magnitude of the velocity in ch1 Co/Pt multilayers [41] and also that of the experiment in Co/Cu(001) films [42]. Because the kinetic energy is proportional to the velocity, the electron must heat up. If we include the band structure of a solid, it will stimulate both intraband and interband transitions [43], leading to demagnetization and magnon generation [44]. We see that the final x is close to zero, so the electron heating is local, the local heating. For clarity, in Fig. 2(b) we shift x by one unit down.

The velocity along the z axis, v_z, is very different. Figure 2(c) shows v_z is always positive, and increases with time, without oscillation. It reaches 1.65×10^{-2} Å/fs. The positivity of v_z, regardless of the type of charge, is crucial to the electron transport, and can be understood from the directions of $\mathbf{E}$ and $\mathbf{B}$. Suppose at one instant of time, $\mathbf{E}$ is along the $+x$ axis and $\mathbf{B}$ along the $+y$ axis. The electron experiences a negative force along the $-x$ axis and gains the velocity along the $-x$ axis, so the Lorentz force due to $\mathbf{B}$ is along the $+z$ direction. Now suppose at another instance, $\mathbf{E}$ changes to $-x$ and $\mathbf{B}$ to $-y$, so the electron velocity is along $+x$, but the Lorentz force is still along the $+z$ axis. If we have a positive charge, the situation is the same. The fundamental reason why we always have a positive force is because the light propagates along the $+z$ axis and the Poynting vector is always along $+z$ and $\mathbf{v} \times \mathbf{B}$ points along the $+z$ axis. We test it with various laser parameters and do not find a negative v_z, in agreement with Gao [45]. Under cw approximation, Rothman and Boughn [46] gave a simple but approximate expression for the dimensionless $v_z = \frac{1}{2}\left(\frac{\omega_c}{\omega}\right)^2[\cos(\omega t) - 1]^2$, and Hagenbuch [47] gave $p_z = e^2A^2(\tau')/2mc$, both of which are positive. Therefore, both their theories and our numerical results agree

that the axial motion of the electron is delivered by both $\mathbf{E}$ and $\mathbf{B}$. This is also consistent with the radiation pressure from a laser beam can accelerate and trap particles [48, 49]. Figure 2(d) shows that z reaches 1.66 Å at 100 fs. Naturally, the electron can move further as time goes by until it collides with other electrons and ions.

Keeping the rest of laser parameters unchanged, i.e., $h\nu = 1.55$ eV and $\tau = 14$ fs, we increase the laser field amplitude A_0 from 0.02 to 0.30 V/Å. Figure 3(a) shows the final velocity as a function of A_0. We notice that v_z change is highly nonlinear. We fit it to a quadratic function, $v_z = \alpha A_0^2$, where α is a constant of 0.383898 Å/(fsV/Å)^2, and find that the fit is almost perfect. Because $|A_0|^2$ is directly proportional to the fluence, this demonstrates v_z is linearly proportional to the laser fluence, which is exactly expected from the Poynting vector $\mathbf{S} = \mathbf{E} \times \mathbf{B}/c$. Thus, both qualitatively and quantitatively our results can be understood. Since the displacement z follows the velocity, it also increases with A_0 quadratically (see Fig. 3(b)).

With growing interest in THz pulses, we investigate the photon energy dependence of v_z and z. We increase $h\nu$ from 0.2 up to 1.6 eV, while keeping both the duration $\tau = 14$ fs and amplitude $A_0 = 0.207$ V/Å fixed. Figure 3(c) shows an astonishing result: both v_z and z are inversely proportional to $h\nu$. At the lower end of $h\nu$, v_z reaches 0.136 Å/fs and z reaches 13.34 Å (see Fig. 3(d)). Note that at such a low amplitude, a pulse of 1.6 eV only drives the electron by 1.60 Å. This explains why THz pulses become a new frontier for ultrafast demagnetization [50–52]. Polley *et al.* [53] employed a THz pulse to demagnetize CoPt films with a goal toward ultrafast ballistic switching. Shalaby *et al.* [54] showed that extreme THz fields with fluence above 100 mJ/cm^2 can induce a significant magnetization dynamics in Co, where the magnetic field becomes more important. ch4 Very recently, using multicycle 2.5-THz pulses, Riepp *et al.* [55] reported incoherent and coherent magnetization dynamics in labyrinth-type Co/Pt multilayers. ch4end Our result uncovers an important picture. When the pulse oscillates more slowly, the electron gains more grounds. Of course, a DC current can move electrons even further, but then it does not have enough field intensity. This result can be tested experimentally.

A. Comparison with prior theories

To the best of our knowledge, there has been no investigation using the experimental laser parameters [29] as we did, so we decide to compare our results with that of Compton scattering. This comparison is possible because we use a free-electron model.

Assume that the initial kinetic energy of the electron is zero. The kinetic energy gained from the photon must be equal to the loss in the photon energy as

$$\frac{1}{2}m_e v_e^2 = Nh\Delta\nu, \rightarrow v_e = \sqrt{\frac{2Nh\Delta\nu}{m_e}} \qquad (8)$$

where v_e is the electron velocity, N is the number of photons that interact with the electron and $\Delta\nu$ is the frequency change computed from the wavelength change $\Delta\lambda$ as $\Delta\nu = -\frac{c}{\lambda^2}\Delta\lambda$. The wavelength change is $\Delta\lambda = \frac{h}{m_e c}(1-\cos\theta)$, where θ is the outgoing angle of the photon with respect to the incident direction (see Fig. 1(b)). We directly compute the velocity of the electron as

$$v_e = \sqrt{\frac{2Nh\Delta\nu}{m_e}} = \frac{h}{m_e\lambda}\sqrt{2N(1-\cos\theta)}. \qquad (9)$$

If we use Brorson's experimental wavelength, we find $v_e = 1.1544 \times 10^3\sqrt{2N(1-\cos\theta)}$ m/s. Except that we have an enormously large N, the electron velocity is around 10^3 m/s. Figure 2(c) shows the final velocity is 1.65×10^{-2} Å/fs or 1.65×10^3 m/s. Therefore, both approaches agree with each other very well.

B. Comparison with experiments

Although Razdolski et al. [29] estimated the axial displacement on the order of 2 nm, it is harder to compare because it depends on the relaxation time of the electron in a particular material. Instead, majority of experiments measured the velocity. Brorson [5] gave $v_e = 1 \times 10^6$ m/s for Au. Melnikov [6] found that a delay of 40 fs for a 50 nm of Au, so the velocity is 1.25×10^6 m/s.

These velocities are three orders of magnitude larger than our theoretical value above. This shows that although our model does yield the correct direction of the electron motion, the free electron model, which is sufficient for atomic and plasma physics, is not adequate for metals, at least for the transport property induced by laser. In the following, we discuss several possible solutions for future research.

IV. BEYOND THE FREE-ELECTRON MODEL

Given the above finding, it is very appropriate to discuss a few alternative theories, as they are crucial to experiments [25].

A. Drude model

We recall first that in metals, the Drude model is often used for the electric transport, where a voltage bias is applied along the longitudinal direction. If an electric field E (constant) is along the x direction, the electron momentum change is given as $\frac{P_f - P_i}{\Delta t} = -eE$, which will grow with time infinitely. Drude realized that the electron must experience collisions from other electrons and ions, so the electron will lose its momentum, whose value is given by $m_e v_d/\tau$. At equilibrium, these two must be equal, so the drift velocity is $v_d = -\frac{eE\tau}{m_e}$, where τ is the

relaxation time, not to be confused with the above laser pulse duration. v_d in metals is around 0.1 m/s [56].

In laser excitation, there is no such field. It is possible to include the magnetic field into the Drude model, but as seen above, this will lead to the same conclusion as our free electron model.

B. Diffusion transport

Diffusion transport has been proposed to understand the electron transport. However, there is a shortcoming in these theories. They do not specify how these initial gradients are established. For instance, Choi et al. [7, 57] and Fognini et al. [58] replaced the particle density n by the chemical potential as $\frac{\partial\mu_s}{\partial t} = D\frac{\partial^2\mu_s}{\partial z^2} - \frac{\mu_s}{\tau_s}$, where $\mu_s = \mu_\uparrow - \mu_\downarrow$ is the spin chemical potential and D is the spin diffusion constant, and τ_s is the spin relaxation time. How a nonzero $\frac{\partial^2\mu_s}{\partial z^2}$ appears is not given. This is also true for the superdiffusion model [17], where the initial velocity of the electron is considered as an input parameter and is not possible to compare with the experimental velocity.

C. Boltzmann equation

The third possibility is to use the Boltzmann equation. The distribution function, $f(\mathbf{r}, \mathbf{v}, t)$, under the influence of the laser field, changes as [59–61]

$$\frac{\partial f}{\partial t} = \lim_{dt\to 0}\frac{f(\mathbf{r}, \mathbf{v}, t) - f(\mathbf{r}, \mathbf{v}, t - dt)}{dt} = -\mathbf{v}\cdot\nabla_\mathbf{r}f - \dot{\mathbf{k}}\cdot\nabla_\mathbf{k}f, \qquad (10)$$

where $\dot{\mathbf{k}} = -\frac{e}{\hbar}(\mathbf{E} + \mathbf{v}\times\mathbf{B})$. We are only interested in k_z because this is along the axial direction, $\dot{k_z} = -ev_x B_y/\hbar$. Since we already know v_x and B_y, we can compute it easily. Figure 4(a) shows how k_z changes with time. We see that Δk_z is very small, whose largest value is around 1.5×10^{-3}Å^{-1}. However, it is sufficient to move electrons in solids. We take fcc Ni as an example. Figure 4(b) shows the band structure of fcc Ni along the Γ-Z direction. There are five bands across the Fermi energy. Regardless of how small Δk_z is, the laser field is able to lift electrons from an occupied band to an unoccupied band, i.e., the intraband transition [43]. Now the questions is whether we have enough photons.

We can estimate the number of photons on the surface of a unit cell from the experiments. We take bcc Fe as an example. Its lattice constant is $a = 2.861$Å, so its cross section is a^2. The experimental fluence [6] is $F = 1$ mJ/cm^2 and the photon energy is $h\nu = 1.55$ eV, so the number of photons per unit cell is 3.296. One bcc cell has two Fe atoms, so each Fe atom receives $n = 1.65$ photons. If we assume that these photons are absorbed, $nh\nu = \frac{1}{2}m_e v_e^2$, we find $v_e = 1.044 \times 10^6$ m/s. For fcc Au, using Brorson's experimental data, we find the number of photons per unit cell to be 5.2746. Each Au atom receives

1.32 photons. We find $v_e = 0.956 \times 10^6$ m/s, which agrees with the experimental value of 10^8 cm/s almost perfectly. Therefore, we believe that it is very likely that a quantum theory, which includes the magnetic field and the band structure, will be able to explain experimental results quantitatively.

V. AFTER INITIAL EXCITATION: RESISTIVE TRANSPORT THEORY

Once electrons have enough velocity, they will travel through the materials [5]. There are three different theories for transport. Ballistic and diffusive transports are two traditional ones [62, 63]. But their separation has not been very clear. In 1998, Bron *et al.* [64] concluded that "the transport of quasi-electrons arriving at the peaks is neither purely ballistic nor purely diffusive". This unclear region is termed the superdiffusive transport [17], but its physics remains unclear. The reason is that for a long time, there have been very few thickness dependence experiments, besides those earlier ones [5, 6, 31, 65]. Heckschen *et al.* [30] carried out a systematic time-resolved two-photon photoemission (2PPE) measurement as a function of the thickness d of Au films from 5 to 105 nm in the Au/Fe/MgO structure. The thickness of Fe is fixed at 7 nm. 2PPE employs two laser pulses. The pump pulse hits on the back of the iron film through the MgO substrate and pushes electrons toward the interface between Fe and Au layers. These hot electrons pass through the interface and enter the Au layer. Once they reach the surface of Au, a probe pulse of 4 eV knocks them out. Experimentally, Heckschen *et al.* collected the electrons as a function of kinetic energy after each time delay between the pump and probe. At $E - E_F = 0.6$ eV, where E is the electron energy and E_F is the Fermi energy, they obtained an accurate dependence of the reduced time delay t^* (see their paper for detail) as a function of d. We use Webdigitizer [66] to read off their experimental data from their Fig. 4 and reproduce them in Fig. 4(c), without error bars. According to their analysis, they found that the dependence of time t on d is sublinear, and concluded that the velocity follows a linear behavior.

However, this concave curve looks strangely familiar to us. In particular, it is not linear, in contrast to the wavelike heat transport [67]. Instead it is more like a function as

$$t = c_0 + \sqrt{c_0^2 + c_1 d}, \qquad (11)$$

where we use t instead of their t^* for simplicity, c_0 and c_1 are two fitting parameters. A quick test indeed confirms our guess, where $c_0 = -4.14678$ fs and $c_1 = 136.398$ fs^2/nm. The fitted data is the solid red line in Fig. 4(c). The match is excellent, given that we only have two fitting parameters and have the experimental errors. The reader must wonder why we only need two fitting parameters, instead of three, which would appear more natural.

This is because we do not have a prior bias toward ballistic, superdiffusive or diffusive transport. We just want to see where the experiment leads us to. We can rewrite Eq. 11 as

$$d = -\frac{2c_0}{c_1}t + \frac{1}{c_1}t^2, \qquad (12)$$

which is a parabola.

This reminds us the motion with a constant acceleration. Consider a one-dimensional motion. The displacement is

$$\Delta x = v_i t + \frac{1}{2}a t^2, \qquad (13)$$

where a is the acceleration, Δx is the same as d above, v_i is the initial velocity. t is the time which may differ from the experimental one (see above and also below). However, in the photoemission, electrons are collected at a fixed kinetic energy, so its final velocity v_f remains the same. We need to replace v_i by v_f as

$$\Delta x = (v_f - at)t + \frac{1}{2}a t^2 = v_f t - \frac{1}{2}a t^2, \qquad (14)$$

which is a crucial step as will be seen below. Comparing Eqs. 12 and 14, we find $a = -2\frac{1}{c_1} = -0.00733nm/fs^2 < 0$. This suggests that electrons inside the Au film deaccelerate under a uniform drag from the ions and other electrons. So it is neither ballistic, nor superdiffusive, nor diffusive. We call it electron resistive transport. The final velocity, $v_f = -\frac{2c_0}{c_1} = 0.0608$ nm/fs, appears too small if we take 0.6 eV as the electron kinetic energy, probably because their time t^* is not an absolute time, as they called it the propagation time [30]. A single agreement is not enough to establish that the uniform drag is indeed the underlying mechanism for electron transports under laser excitation. We move on to the Brorson's data [5], but unfortunately there is not enough data within 150 nm (they only have two points).

Fortunately, Suarez *et al.* [31] have three data points below and above 150 nm. We obtain the data using Webdigitizer [66] from the inset of their Fig. 1 and reproduce their data in 4(d) (see three empty circles and boxes). In their original paper, they linked all six data points together and used a straight line to fit their data to suggest a possible ballistic transport, because they noticed that the time "does not vary as the second power of the film thickness as one would expect from random-walk thermal diffusion". The red short-dashed line is our fitted curve $t = c_0 + \sqrt{c_0^2 + c_1 d}$, where $c_0 = -239.382$ fs and $c_1 = 585.481$ fs^2/nm. The fitting is quite good as well, given that they only have three data points. What is more important that it has the same trend as Heckschen's data (the thin solid line from Fig. 4(c) is reproduced in Fig. 4(d)). Caution must be taken to make a quantitative comparison. Suarez's time is the traversal time which is defined as the transient reflectivity reaches 15%. From c_0 and c_1, we find $a = -0.0034$ nm/fs^2 and $v_f = 0.82$ nm/fs.

We see both accelerations have the same magnitude, but their velocities differ. Suarez's velocity is closer to the Fermi velocity. More experimental data are necessary.

To investigate whether our theory can reproduce the ballistic limit, we rewrite Eq. 14 as

$$\frac{1}{2}at^2 - v_f t + \Delta x = 0, \tag{15}$$

so the time t is given by

$$t(\Delta x) = \frac{v_f \pm \sqrt{v_f^2 - 2a\Delta x}}{a}, \tag{16}$$

which reveals immediately why we must only have two fitting parameters for a Δx. Since v_f and Δx are both positive, we only choose a root for a positive t, which avoids the complex math if we used v_i. In our resistive transport, $a < 0$, so the numerator must be negative as well. Therefore we choose a negative sign in the numerator,

$$t(\Delta x) = \frac{v_f - \sqrt{v_f^2 - 2a\Delta x}}{a}. \tag{17}$$

To reproduce the ballistic limit, we expand the square root in Eq. 17 by using $\sqrt{1 \pm x} = 1 \pm \frac{1}{2}x - \frac{1}{2}\frac{1}{4}x^2 + \cdots$ to find,

$$t(\Delta x) = \frac{\Delta x}{v_f} + \frac{a(\Delta x)^2}{2v_f^3} + \cdots. \tag{18}$$

If we drop the second and other higher order terms, we get the ballistic limit $t(\Delta x) = \frac{\Delta x}{v_f}$. According to the anomalous multiphoton photoelectric measurement [68], the photoelectron current has a dramatic enhancement when the gold overlayer thickness is nearly 43 nm, i.e., right in the middle of the resistive transport. This anomalous effect is likely due to the resistive transport (see Fig. 4(d)). Interestingly, Kupersztych and Raynaud [68] already stated that "electromagnetic energy is transferred ... to conduction electrons in a duration less than the electron energy damping time". This damping now shows up in our negative acceleration.

We can estimate how much the electron velocity is reduced. Using $a = -0.0034$ nm/fs^2, every additional 100 fs, the velocity is reduced by 0.34 nm/fs. As the electrons slow down, they start to accumulate spatially, ready for a normal diffusion. The resistive transport transitions to the regular diffusion (see Fig. 4(d)). We fit Suarez's data (last three points) to $t(d) = g_0 + g_1 d^2$, where $g_0 = 88.2088$ fs and $g_1 = 0.00238099$ fs/nm^2. A spatial separation between the resistive and diffusive transports in Au is around 200 nm as seen from Fig. 4(d). The reason why our simple resistive picture works well is because the interband state in Au is roughly 3 eV above E_F [31, 69] and the transport is strictly due to intraband transition [43]. This may be different for different materials [70]. We are also aware of a similar concave down in the size dependence of the electron thermalization time for nanoparticles [71, 72], but the dependence is unlikely related to the electron velocity, since its value is too small.

VI. CONCLUSION

This study centers on two key themes. First we have shown that the electron axial transport is the joint effect of the electric and magnetic fields of the laser pulse. Each field alone cannot lead to the transport along the axial direction. The electric field provides a strong transverse velocity, while the magnetic field steers the electron moving along the light propagation direction. This welcoming result requires a nonzero $\mathbf{B}$, but a nonzero $\mathbf{B}$ subsequently requires a spatially dependent vector potential $\mathbf{A}(\mathbf{r}, t)$, owing to $\mathbf{B} = \nabla \times \mathbf{A}(\mathbf{r}, t)$. The dipole approximation is frequently employed in model and first-principles theories [73–76], but in order to describe electron transports in thin films, one has to adopt $\mathbf{A}(\mathbf{r}, t)$, not $\mathbf{A}(t)$. However, quantitatively, our free-electron model is still unable to reproduce the experimental velocity. Going beyond the free electron model, if all the photon energies are absorbed, we can quantitatively reproduce the experimental velocity. Second, by carefully analyzing the experimental data, we propose a concept of the resistive transport, which unifies the ballistic and superdiffusive transports. Here electrons, after initial acceleration by the laser pulse, deaccelerate under a uniform resistance from other electrons and ions. Earlier part of the resistive transport is the ballistic transport, while the later part covers superdiffusive transport. As electrons slow down, they enter a normal diffusion regime. Our study provides a much simpler picture on the ultrafast time scale, and reveals a big deficiency with the existing theories [23, 24, 35, 36, 77]. ch3A new experiment is now available in copper. Jechumtal *et al.* [78] unknowingly reported a similar square-root dependence. They thought that because of the limitation of their model, the model does not capture the slightly nonlinear trend in their Figs. 3(a) and 3(b) for the thickness $d < 3$ nm. They even put a shaded triangle over the nonlinear portion of the curve. Now, this is in fact the result of the resistive transport, another proof of our theory.

* guo-ping.zhang@outlook.com. https://orcid.org/0000-0002-1792-2701

The data that support the findings of this study are available from the corresponding author upon reasonable

request.

VII. REFERENCES

[1] W. Schäfer and M. Wegener, *Semiconductor Optics and Transport Phenomena*, Springer-Verlag Berlin Heidelberg (2002).

[2] G. D. Mahan, *Many-Particle Physics*, Springer, Boston, MA (2000).

[3] D. M. Riffe and R. B. Wilson, Excitation and relaxation of nonthermal electron energy distributions in metals with application to gold, Phys. Rev. B **107**, 214309 (2023).

[4] S. Datta, Quantum Transport: Atom to Transistor, Cambridge University Press (2005).

[5] S. D. Brorson, J. G. Fujimoto, and E. P. Ippen, Femtosecond electronic heat-transport dynamics in thin gold films, Phys. Rev. Lett. **59**, 1962 (1987).

[6] A. Melnikov, I. Razdolski. T. O. Wehling, E. Th. Papaioannou, V. Roddatis, P. Fumagalli, O. Aktsipetrov, A. I. Lichtenstein, and U. Bovensiepen, Ultrafast transport of laser-excited spin-polarized carriers in Au/Fe/MgO(001), Phys. Rev. Lett. **107**, 076601 (2011).

[7] G.-M. Choi, B.-C. Min, K.-J. Lee and D. G. Cahill, Spin current generated by thermally driven ultrafast demagnetization, Nat. Comm. **5**, 4334 (2014).

[8] B. Vodungbo, J. Gautier, G. Lambert, A. B. Sardinha, M. Lozano, S. Sebban, M. Ducousso, W. Boutu, K. Li, B. Tudu, M. Tortarolo, R. Hawaldar, R. Delaunay, V. Lopez-Flores, J. Arabski, C. Boeglin, H. Merdji, P. Zeitoun, and J. Lüning, Laser-induced ultrafast demagnetization in the presence of a nanoscale magnetic domain network, Nat. Commun. **3**, 999 (2012).

[9] B. Pfau, S. Schaffert, L. Müller, C. Gutt, A. Al-Shemmary, F. Büttner, R. Delaunay, S. Düsterer, S. Flewett, R. Frömter, J. Geilhufe, E. Guehrs, C. M. Günther, R. Hawaldar, M. Hille, N. Jaouen, A. Kobs, K. Li, J. Mohanty, H. Redlin, W.F. Schlotter, D. Stickler, R. Treusch, B. Vodungbo, M. Klüi, H. P. Oepen, J. Lüning, G. Grüel and S. Eisebitt, Ultrafast optical demagnetization manipulates nanoscale spin structure in domain walls, Nat. Commun. **3**, 1100 (2012).

[10] J. Kimling and D. G. Cahill, Spin diffusion induced by pulsed-laser heating and the role of spin heat accumulation, Phys. Rev. B **95**, 014402 (2017).

[11] M. Hofherr, P. Maldonado, O. Schmitt, M. Berritta, U. Bierbrauer, S. Sadashivaiah, A. J. Schellekens, B. Koopmans, D. Steil, M. Cinchetti, B. Stadtmüller, P. M. Oppeneer, S. Mathias, and M. Aeschlimann, Speed and efficiency of femtosecond spin current injection into a nonmagnetic material, Phys. Rev. B **96**, 100403(R) (2017).

[12] T. Seifert, U. Martens, S. Günther, M. A. W. Schoen, F. Radu, X. Z. Chen, I. Lucas, R. Ramos, M. H. Aguirre, P. A. Algarabel, A. Anadon, H. S. Körner, J. Walowski, C. Back, M. R. Ibarra, L. Morellon, E. Saitoh, M. Wolf, C. Song, K. Uchida, M. Münzenberg, I. Radu and T. Kampfrath, Terahertz spin currents and inverse spin Hall effect in thin-film heterostructures containing complex magnetic compounds, SPIN **7**, 1740010 (2017).

[13] T. S. Seifert, N. M. Tran, O. Gueckstock, S. M. Rouzegar, L. Nadvornik, S. Jaiswal, G. Jakob, V. V. Temnov, M. Müzenberg, M. Wolf, M. Kläui and T. Kampfrath, Terahertz spectroscopy for all-optical spintronic characterization of the spin-Hall-effect metals Pt, W and $Cu_{80}Ir_{20}$, J. Phys. D: Appl. Phys. **51**, 364003 (2018)

[14] J. Chen, U. Bovensiepen, A. Eschenlohr, T. Müller, P. Elliott, E. K. U. Gross, J. K. Dewhurst, and S. Sharma, Competing spin transfer and dissipation at Co/Cu(001) interfaces on femtosecond timescales, Phys. Rev. Lett. **122**, 067202 (2019).

[15] Y. Beyazit, J. Beckord, P. Zhou, J. P. Meyburg, F. Küne, D. Diesing, M. Ligges, and U. Bovensiepen, Local and Nonlocal electron dynamics of Au/Fe/MgO heterostructures analyzed by time-resolved two-photon photoemission spectroscopy, Phys. Rev. Lett. **125**, 076803 (2020).

[16] Y. Beyazit, F. Kühne, D. Diesing, P. Zhou, J. Jayabalan, B. Sothmann, and U. Bovensiepen, Ultrafast electron dynamics in Au/Fe/MgO(001) analyzed by Au- and Fe-selective pumping in time-resolved two-photon photoemission spectroscopy: Separation of excitations in adjacent metallic layers, Phys. Rev. B **107**, 085412 (2023).

[17] M. Battiato, K. Carva, and P. M. Oppeneer, Theory of laser-induced ultrafast superdiffusive spin transport in layered heterostructures, Phys. Rev. B **86**, 024404 (2012).

[18] F. Kühne, Y. Beyazit, B. Sothmann, J. Jayabalan, D. Diesing, P. Zhou, and U. Bovensiepen, Ultrafast transport and energy relaxation of hot electrons in Au/Fe/MgO(001) heterostructures analyzed by linear time-resolved photoelectron spectroscopy, Phys. Rev. Res. **4**, 033239 (2022).

[19] K. Bühlmann, G. Saerens, A. Vaterlaus, and Y. Acremann, Detection of femtosecond spin injection into a thin gold layer byÂ time and spin resolved photoemission, Sci. Rep. **10**, 12632 (2020).

[20] P. Karna, M. S. Bin Hoque, S. Thakur, P. E. Hopkins, and A. Giri, Direct measurement of ballistic and diffusive electron transport in gold, Nano Lett. **23**, 491 (2023).

[21] J. Hohlfeld, S.-S. Wellershoff, J. Güdde, U. Conrad, V. Jähnke and E. Matthias, Electron and lattice dynamics following optical excitation of metals, Chem. Phys. **251**, 237 (2000).

[22] G. Salvatella, R. Gort, K. Bühlmann, S. Däster, A. Vaterlaus, Y. Acremann, Ultrafast demagnetization by hot electrons: Diffusion or super-diffusion? Struct. Dyn. **3**, 055101 (2016).

[23] B. Liu, H. Xiao, and M. Weinelt, Microscopic insights to spin transport driven ultrafast magnetization dynamics in a Gd/Fe bilayer, Sci. Adv. **9**, eade0286(2023).

[24] K. Kang, H. Omura, D. Yesudas, O. Lee, K.-J. Lee, H.-W. Lee, T. Taniyama, and G.-M. Choi, Spin current driven by ultrafast magnetization of FeRh, Nat. Commun. **14**, 3619 (2023).

[25] G. Malinowski, N. Bergeard, M. Hehn, and S. Mangin, Hot-electron transport and ultrafast magnetization dynamics in magnetic multilayers and nanostructures following femtosecond laser pulse excitation, Eur. Phys. J. B **91**, 98 (2018).

[26] J. H. Yang, R. S. Craxton, and M. G. Haines, Explicit general solutions to relativistic electron dynamics in plane-wave electromagnetic fields and simulations of pondermotive acceleration, Plasma Phys. Control. Fusion **53**, 125006 (2011).

[27] J. Maurer and U. Keller, Ionization in intense laser fields beyond the electric dipole approximation: concepts, methods, achievements and future directions, J. Phys. B: At. Mol. Opt. Phys. **54**, 094001 (2021).

[28] H. Jang, J. Kimling, and D. G. Cahill, Nonequilibrium heat transport in Pt and Ru probed by an ultrathin Co thermometer, Phys. Rev. B **101**, 064304 (2020).

[29] I. Razdolski, A. Alekhin, N. Ilin, J. P. Meyburg, V. Roddatis, D. Diesing, U. Bovensiepen, and A. Melnikov, Nanoscale interface confinement of ultrafast spin transfer torque driving non-uniform spin dynamics, Nat. Comm. **8**, 15007 (2017).

[30] M. Heckschen, Y. Beyazit, E. Shomali, F. Kühne, J. Jayabalan, P. Zhou, D. Diesing, M. E. Gruner, R. Pentcheva, A. Lorke, B. Sothmann, and U. Bovensiepen, Spatio-temporal electron propagation dynamics in Au/Fe/MgO(001) in nonequilibrium: Revealing single scattering events and the ballistic limit, PRX ENERGY **2**, 043009 (2023).

[31] C. Suarez, W. E. Bron, and T. Juhasz, Dynamics and transport of electronic carriers in thin gold films, Phys. Rev. Lett. **75**, 4536 (1995).

[32] Q. Xiong and X. Tian, Effect of ballistic electrons on ultrafast thermomechanical responses of a thin metal film, Chin. Phys. B **26**, 096501 (2017).

[33] A. Suslova and A. Hassanein, Numerical simulation of ballistic electron dynamics and heat transport in metallic targets exposed to ultrashort laser pulse, J. App. Phys. **124**, 065108 (2018).

[34] C. D. Stanciu, F. Hansteen, A. V. Kimel, A. Kirilyuk, A. Tsukamoto, A. Itoh, and Th. Rasing, All-optical magnetic recording with circularly polarized light, Phys. Rev. Lett. **99**, 047601 (2007).

[35] G. P. Zhang, M. Murakami, M. S. Si, Y. H. Bai, and T. F. George, Understanding all-optical spin switching: Comparison between experiment and theory, Mod. Phys. Lett. B **32**, 1830003 (2018).

[36] G. P. Zhang, R. Meadows, A. Tamayo, Y. H. Bai, and T. F. George, An attempt to simulate laser-induced all-optical spin switching in a crystalline ferrimagnet, AIP Adv. **10**, 125323 (2020).

[37] D. J. Griffiths and D. F. Schroeter, *Introduction to quantum mechanics*, Cambridge University Press, 3rd edition, page 182 (2018).

[38] P. Varga and P. Török, The Gaussian wave solution of Maxwell's equations and hte validity of scalar wave approximation, Opt. Commun. **152**, 108 (1998).

[39] M. S. Si and G. P. Zhang, Resolving photon-shortage mystery in femtosecond magnetism, J. Phys.: Condens. Matter **22**, 076005 (2010).

[40] G. P. Zhang, G. Lefkidis, M. Murakami, W. Hübner, and T. F. George, *Introduction to Ultrafast Phenomena: From Femtosecond Magnetism to High-Harmonic Generation*, CRC Press, Taylor & Francis Group, Boca Raton, Florida (2021).

[41] N. Bergeard, M. Hehn, S. Mangin, G. Lengaigne, F. Montaigne, M. L. M. Lalieu, B. Koopmans, and G. Malinowski, Hot-electron-induced ultrafast demagnetization in Co/Pt multilayers, Phys. Rev. Lett. **117**, 147203 (2016).

[42] J. Wieczorek, A. Eschenlohr, B. Weidtmann, M. Rösner, N. Bergeard, A. Tarasevitch, T. O. Wehling, and U. Bovensiepen, Separation of ultrafast spin currents and spin-flip scattering in Co/Cu(001) driven by femtosecond laser excitation employing the complex magneto-optical Kerr effect, Phys. Rev. B **92**, 174410 (2015).

[43] M. Murakami and G. P. Zhang, Strong ultrafast demagnetization due to the intraband transitions, J. Phys.: Condens. Matter **35**, 495803 (2023).

[44] G. P. Zhang, M. Murakami, Y. H. Bai, T. F. George, and X. S. Wu, Spin-orbit torque-mediated spin-wave excitation as an alternative paradigm for femtomagnetism, J. Appl. Phys. **126**, 103906 (2019).

[45] J. Gao, Thomson scattering from ultrashort and ultraintense laser pulses, Phys. Rev. Lett. **93**, 243001 (2004).

[46] T. Rothman and S. Boughn, The Lorentz force and the radiation pressure of light, Am. J. Phys. **77**, 122 (2009).

[47] K. Hagenbuch, Free electron motion in a plane electromagnetic wave, Am. J. Phys. **45**, 693 (1977).

[48] A. Ashkin, Acceleration and trapping of particles by radiation pressure, Phys. Rev. Lett. **24**, 156 (1970).

[49] A. Ashkin, J. M. Dziedzic, J. E. Bjorkholm, and S. Chu, Observation of a single-beam gradient force optical trap for dielectric particles, Opt. Lett. **11**, 288 (1986).

[50] M. Shalaby, C. Vicario, and C. P. Hauri, The terahertz frontier for ultrafast coherent magnetic switching: Terahertz-induced demagnetization of ferromagnets, arxiv.org/abs/1506.05397.

[51] M. Hudl, M. d'Aquino, M. Pancald, S.-H. Yang, M. G. Samant, S. S. P. Parkin, H. A. Dürr, C. Serpico, M. C. Hoffmann, and S. Bonetti, Nonlinear magnetization dynamics driven by strong terahertz fields, Phys. Rev. Lett. **123**, 197204 (2019).

[52] H. Lee, C. Weber, M. Fähnle and M. Shalaby, Ultrafast electron dynamics in magnetic thin films, Appl. Sci. **11**, 9753 (2021).

[53] D. Polley, M. Pancaldi, M. Hudl, P. Vavassori, S. Urazhdin and S. Bonetti, THz-driven demagnetization with perpendicular magnetic anisotropy: towards ultrafast ballistic switching, J. Phys. D: Appl. Phys. **51**, 084001 (2018).

[54] M. Shalaby, A. Donges, K. Carva, R. Allenspach, P. M. Oppeneer, U. Nowak, and C. P. Hauri, Coherent and incoherent ultrafast magnetization dynamics in 3d ferromagnets driven by extreme terahertz fields, Phys. Rev. B **98**, 014405 (2018).

[55] M. Riepp, A. Philippi-Kobs, L. Müller, W. Roseker, R. Rysov, R. Frömter, K. Bagschik, M. Hennes, D. Gupta, S. Marotzke, M. Walther, S. Bajt, R. Pan, T. Golz, N. Stojanovic, C. Boeglin, and G. Grübel, Terahertz-driven coherent magnetization dynamics in labyrinth-type domain networks, Phys. Rev. B **110**, 094405 (2024).

[56] H. C. Ohanian, *Modern Physics*, Prentice Hall, Upper Saddle River, NJ 07458.

[57] G.-M. Choi and D. G. Cahill, Kerr rotation in Cu, Ag, and Au driven by spin accumulation and spin-orbit coupling, Phys. Rev. B **90**, 214432 (2014).

[58] A. Fognini, T. U. Michlmayr, A. Vaterlaus and Y. Acremann, Laser-induced ultrafast spin current pulses: a thermodynamic approach, J. Phys.: Condens. Matter **29**, 214002 (2017).

[59] R. B. Thomas, Magnetic corrections to the Boltzmann transport equation, Phys. Rev. **152**, 138 (1966).

[60] C. Kittel, *Introduction to Solid State Physics*, 7th Ed., John Wiley & Sons, Inc., New York (1996).

[61] G. D. Mahan, Quantum transport equation for electric and magnetic fields, Physics Reports **145**, 251 (1987).

[62] R. Knorren, G. Bouzerar and K. H. Bennemann, Theory for the dynamics of excited electrons in noble and transition metals, J. Phys.: Condens. Matter **14**, R739 (2002).

[63] W.-L. Chan,· R. S. Averback and D. G. Cahill, Nonlinear energy absorption of femtosecond laser pulses in noble metals, Appl. Phys. A **97**, 287 (2009).

[64] W. E. Bron, A. Guerra III, and C. Suarez, Quasi-electron and phonon interactions in the femtosecond time domain J. Lumin. **76/77**, 518 (1998).

[65] T. Juhasz, H. E. Elsayed-Ali, G. O. Smith, C. Suarez, and W. E. Bron, Direct measurements of the transport of nonequilibrium electrons in gold films with different crystal structures, Phys. Rev. B **48**, 15488 (1993).

[66] WebPlotDigitizer, *Web based tool to extract data from plots, images, and maps*, https://automeris.io/WebPlotDigitizer/.

[67] S. L. Sobolev and W. Dai, Heat transport on ultrashort time and space scales in nanosized systems: Diffusive or wave-like?, Materials **15**, 4287 (2022).

[68] J. Kupersztych and M. Raynaud, Anomalous multiphoton photoelectric effect in ultrashort time scales, Phys. Rev. Lett. **95**, 147401 (2005).

[69] X. Liu, R. Stock, and W. Rudolph, Ballistic electron transport in Au films, Phys. Rev. B **72**, 195431 (2005).

[70] A. I. H. Persson, A. Jarnac, X. Wang, H. Enquist, A. Jurgilaitis, and J. Larsson, Studies of electron diffusion in photo-excited Ni using time-resolved X-ray diffraction, Appl. Phys. Lett. **109**, 203115 (2016).

[71] C. Voisin, D. Christofilos, N. Del Fatti, F. Vallee. B. Prevel, E. Cottancin, J. Lermé, M. Pellarin, and M. Broyer, Size-dependent electron-electron interactions in metal nanoparticles, Phys. Rev. Lett. **85**, 2200 (2000).

[72] C. Voisin, N. Del Fatti, D. Christofilos, and F. Vallee, Ultrafast electron dynamics and optical nonlinearities in metal nanoparticles, J. Phys. Chem. B **105**, 2264 (2001).

[73] G. P. Zhang, G. Lefkidis, W. Hübner, and Y. Bai, Ultrafast demagnetization in ferromagnets and magnetic switching in nanoclusters when the number of photons is kept fixed, J. Appl. Phys. **109**, 07D303 (2011).

[74] K. Krieger, J. K. Dewhurst, P. Elliott, S. Sharma, and E. K. U. Gross, Laser-induced demagnetization at ultrashort time scales: Predictions of TDDFT, J. Chem. Theory and Comput. **11**, 4870 (2015).

[75] Z. H. Chen and L. W. Wang, Role of initial magnetic disorder: A time-dependent ab initio study of ultrafast demagnetization mechanisms, Sci. Adv. **8**, eaau8000 (2019).

[76] S. R. Acharya, V. Turkowski, G. P. Zhang, and T. Rahman, Ultrafast electron correlations and memory effects at work: Femtosecond demagnetization in Ni, Phys. Rev. Lett. **125**, 017202 (2020).

[77] Y. Liu, U. Bierbrauer, C. Seick, S. T. Weber, M. Hofherr, N. Y. Schmidt, M. Albrecht, D. Steil, S. Mathias, H. C. Schneider, B. Rethfeld, B. Stadtmüller, and M. Aeschlimann, Ultrafast magnetization dynamics of Mn-doped L1$_0$ FePt with spatial inhomogeneity, J. Magn. Magn. Mater. **502**, 166477 (2020).

[78] J. Jechumtal, R. Rouzegar, O. Gueckstock, C. Denker, W. Hoppe, Q. Remy, T. S. Seifert, P. Kubascik, G. Woltersdorf, P. W. Brouwer, M. Münzenberg, T.
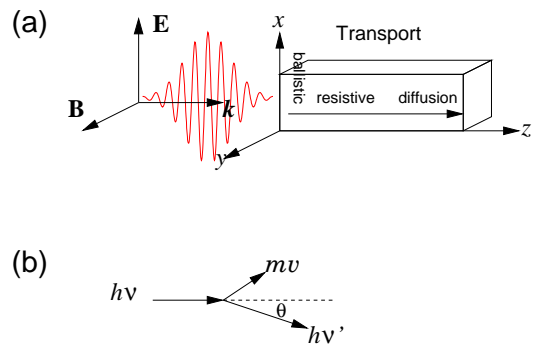
FIG. 1. (a) A linearly polarized laser pulse propagates along the z axis with the wavevector **k**, where the electric field **E** is along the x axis and the magnetic field **B** is along the y axis. Electron transport is separated into two regimes: resistive and diffusive transports. The ballistic transport is in the beginning of the resistive transport. (b) Compton scattering, where a photon comes from the left and collides with a static electron.
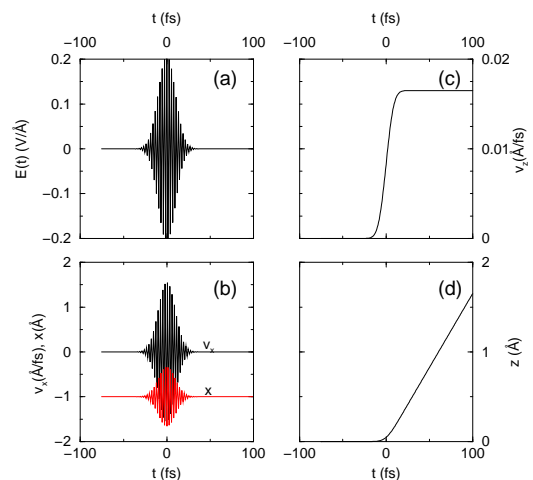

FIG. 2. (a) Electric field of the experimental laser pulse of 14 fs, fluence of 10 mJ/cm^2, and photon energy of 1.55 eV [29]. Here $A_0 = 0.207$ V/Å. (b) The electron velocity v_x and position x oscillate strongly with time. The electron moves little along the x axis. x is downshifted by one unit for clarity. (c) v_z does not oscillate and only increases monotonically with time. (d) z increases with time t.

Kampfrath, and L. Nadvornik, Accessing ultrafast spin-transport dynamics in copper using broadband terahertz spectroscopy, Phys. Rev. Lett. **132**, 226703 (2024).
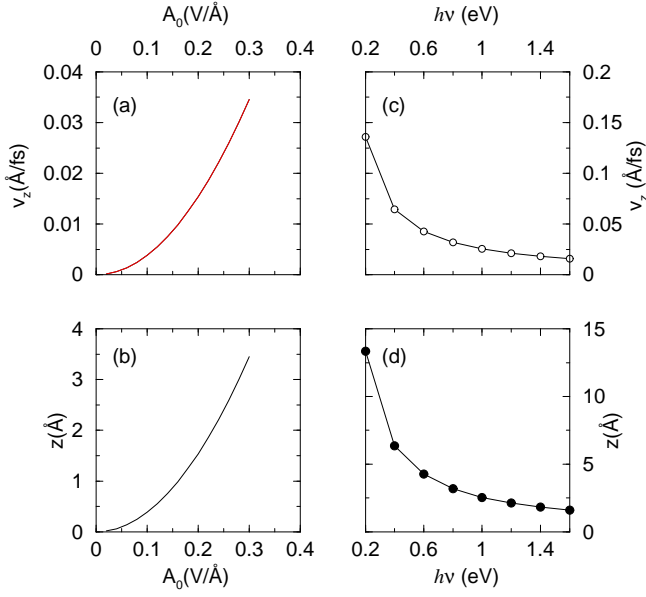
FIG. 3. (a) Final velocity of the electron as a function of the laser amplitude A_0 from 0.02 to 0.30 V/Å, corresponding to the fluence F from 0.09 to 20.96 mJ/cm^2. (b) Final position as a function of A_0. (c) Final velocity of the electron as a function of $h\nu$. (d) Final position of the electron as a function of $h\nu$.
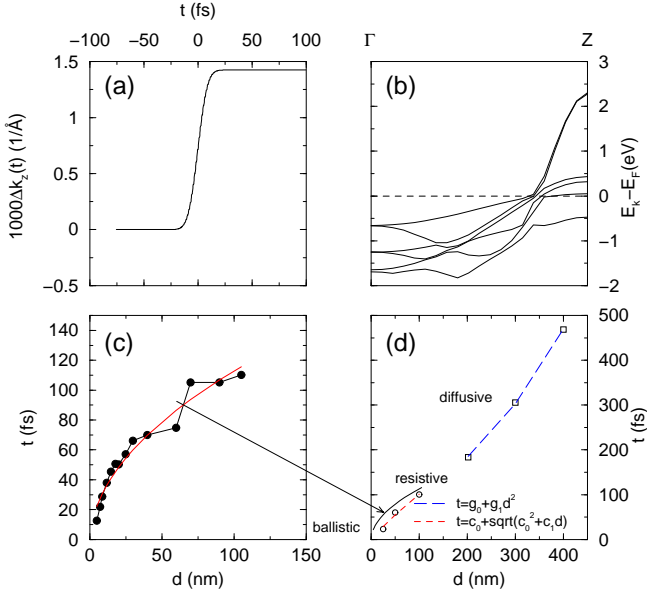

FIG. 4. (a) Wavevector change Δk_z as a function of time. (b) Band structure of fcc Ni along the Γ-Z axis. The horizontal line is the Fermi level. (c) Photoemission data (filled dots) from Heckschen *et al.* [30]. The thin line is our resistive theory prediction, which has a concave down. (d) Experimental data (empty circles and boxes) from Suarez *et al.* [31]. The short dashed line is our resistive transport fit, a typical concave down. The long-dashed line is a fit to the diffusive equation. The thin solid line is from (c) to see how similar both experimental data are.